REPORT DOCUMENTATION PAGE

Form Approved
OMB No. 0704-0188

1. REPORT DATE *(DD-MM-YYYY)*	**2. REPORT TYPE**	**3. DATES COVERED** *(From - To)*
18-01-2007	Journal Article	

4. TITLE AND SUBTITLE

Interior and Exterior Laser-Induced Fluorescence and Plasma Measurements within a Hall Thruster

5a. CONTRACT NUMBER

5b. GRANT NUMBER

5c. PROGRAM ELEMENT NUMBER

6. AUTHOR(S)
W.A. Hargus, Jr. (AFRL/PRSS); M.A. Cappelli (Stanford University)

5d. PROJECT NUMBER
10110009

5e. TASK NUMBER

5f. WORK UNIT NUMBER

7. PERFORMING ORGANIZATION NAME(S) AND ADDRESS(ES)

Air Force Research Laboratory (AFMC)
AFRL/PRSS
1 Ara Drive
Edwards AFB CA 93524-7013

8. PERFORMING ORGANIZATION REPORT NUMBER

AFRL-PR-ED-JA-2007-036

9. SPONSORING / MONITORING AGENCY NAME(S) AND ADDRESS(ES)

Air Force Research Laboratory (AFMC)
AFRL/PRS
5 Pollux Drive
Edwards AFB CA 93524-70448

10. SPONSOR/MONITOR'S ACRONYM(S)

11. SPONSOR/MONITOR'S NUMBER(S)
AFRL-PR-ED-JA-2007-036

12. DISTRIBUTION / AVAILABILITY STATEMENT

Approved for public release; distribution unlimited (AFRL-ERS-PAS-2007-036)

13. SUPPLEMENTARY NOTES
Published in the Journal of Propulsion and Power, 18(1), 159-168 (2002).

14. ABSTRACT

We describe results of a study of emissive-probe-based plasma potential measurements and laser-induced fluorescence velocimetry of neutral and singly ionized xenon in the plume and interior portions of the acceleration channel of a Hall thruster plasma discharge operating at powers ranging from 250 to 725 W. Axial ion and neutral velocity profiles for four discharge voltage conditions (100, 160, 200, and 250V) are measured as are radial ion velocity profiles in the near-field plume. Axial ion velocity measurements both inside and outside the thruster as well as radial velocity measurements outside the thruster are performed using laser-induced fluorescence with nonresonant signal detection. Neutral axial velocity measurements are similarly performed in the interior of the Hall thruster with resonance fluorescence collection. Optical access to the interior of the Hall thruster is provided by a 1-mm-wide axial slot in the outer insulator wall. The majority of the ion velocity measurements used partially saturated fluorescence to improve the signal-to-noise ratio. Probe-based plasma potential measurements extend from 50 mm outside the thruster exit plane to the near anode region for all but the highest discharge voltage condition. For each condition, the axial electric field is calculated from the plasma potential, and the local electron temperature is determined from the difference between the floating and plasma potentials. These two sets of measurements delineate the structure of the plasma and indicate that the ionization and acceleration regions are somewhat separated. Also, these measurements indicate a region of low electric field near the thruster exit, especially at the higher discharge voltages. This region of near constant potential (low electric field) may be a result of oscillations, which enhance the local plasma conductivity.

15. SUBJECT TERMS

16. SECURITY CLASSIFICATION OF:			**17. LIMITATION OF ABSTRACT**	**18. NUMBER OF PAGES**	**19a. NAME OF RESPONSIBLE PERSON**
					Dr. James Haas
a. REPORT	**b. ABSTRACT**	**c. THIS PAGE**	SAR	11	**19b. TELEPHONE NUMBER** *(include area code)*
Unclassified	**Unclassified**	**Unclassified**			N/A

JOURNAL OF PROPULSION AND POWER
Vol. 18, No. 1, January–February 2002

Interior and Exterior Laser-Induced Fluorescence and Plasma Measurements within a Hall Thruster

W. A. Hargus Jr.* and M. A. Cappelli†
Stanford University, Stanford, CA 94305

We describe results of a study of emissive-probe-based plasma potential measurements and laser-induced fluorescence velocimetry of neutral and singly ionized xenon in the plume and interior portions of the acceleration channel of a Hall thruster plasma discharge operating at powers ranging from 250 to 725 W. Axial ion and neutral velocity profiles for four discharge voltage conditions (100, 160, 200, and 250 V) are measured as are radial ion velocity profiles in the near-field plume. Axial ion velocity measurements both inside and outside the thruster as well as radial velocity measurements outside the thruster are performed using laser-induced fluorescence with nonresonant signal detection. Neutral axial velocity measurements are similarly performed in the interior of the Hall thruster with resonance fluorescence collection. Optical access to the interior of the Hall thruster is provided by a 1-mm-wide axial slot in the outer insulator wall. The majority of the ion velocity measurements used partially saturated fluorescence to improve the signal-to-noise ratio. Probe-based plasma potential measurements extend from 50 mm outside the thruster exit plane to the near anode region for all but the highest discharge voltage condition. For each condition, the axial electric field is calculated from the plasma potential, and the local electron temperature is determined from the difference between the floating and plasma potentials. These two sets of measurements delineate the structure of the plasma and indicate that the ionization and acceleration regions are somewhat separated. Also, these measurements indicate a region of low electric field near the thruster exit, especially at the higher discharge voltages. This region of near constant potential (low electric field) may be a result of oscillations, which enhance the local plasma conductivity.

Introduction

BECAUSE of their high specific impulse and thrust efficiencies, Hall thrusters are now being considered for use on commercial, research, and military spacecraft. This technology provides economic advantages for a number of missions, and its use can be translated into lower launch mass, longer time on station, or larger payloads.[1] To extend the performance and operating envelope of Hall thrusters, there is a need for increased understanding of the complex phenomena that control propellant ionization and acceleration within the discharge. To more fully understand the physics in these discharges, several laboratory model Hall thrusters have been constructed at Stanford University. These thrusters serve as test articles for model development and advanced plasma diagnostics including laser-induced fluorescence (LIF), probes of various types, and thrust measurements.[2–4]

Laser-based techniques have been developed to nonintrusively probe neutral and ionized xenon. Such measurements in the plumes of Hall and other types of ion thrusters provide important information on the expansion of the plasma plume and its potential effect on satellite propulsion design and integration. Laser-based diagnostic measurements have been previously employed to examine plume plasma properties in other electric propulsion devices. For example, the hydrogen arcjet has been extensively studied using lasers to measure velocity, temperature, and electron number density.[5] However, few measurements (especially optical measurements) have been made within the interior discharge of these devices.[6] The high spatial resolution of single-point LIF is essential in probing nonuniform plasma environments such as those inside Hall thrusters and other electric propulsion devices.

Both axial ion velocity measurements inside and outside the thruster and radial velocity measurements outside the thruster are performed using LIF with nonresonant signal detection exciting the xenon ion $5d[4]_{7/2}$–$6p[3]_{5/2}$ electronic transition while monitoring the signal from the $6s[2]_{3/2}$–$6p[3]_{5/2}$ transition. Neutral axial velocity measurements are similarly performed in the interior of the Hall thruster using the $6s[\frac{3}{2}]^0_2$–$6p[\frac{3}{2}]_2$ transition with resonance fluorescence collection. The majority of the velocity measurements use partially saturated fluorescence to improve the signal-to-noise-ratio.

Use of emissive plasma potential probes provides near instantaneous measurement of the local plasma potential. With these measurements, the electric field may be calculated by differentiation of the plasma potential field. Measurements of this kind are important because Hall thrusters are electrostatic devices in which propellant ions are accelerated via electric body forces. Although the use of emissive probes is intrusive, it provides a more reliable measurement of the plasma potential than swept langmuir probes when clean electron saturation currents cannot be obtained.

Theory

LIF

The interaction of a laser beam with a plasma involves the optical excitation of a number of atoms, or ions, to higher energy states. The excitation is more likely to occur if the laser is tuned to the energy difference $h\nu_{12}$ between an upper and lower energy level. The interaction can be investigated by either monitoring the resulting reduction in laser power following propagation through the plasma (absorption), or by monitoring the subsequent spontaneous emission as the resulting excited state relaxes to a lower state (LIF). Monitoring the fluorescence as the laser is tuned over the transition provides a measure of the fluorescence excitation line shape and is favored for the higher spatial resolution that it affords in the determination of plasma parameters. The spatial resolution of LIF measurements is determined by the intersection of the probe laser beam with the optical collection volume.

Received 10 July 2000; revision received 23 April 2001; accepted for publication 24 May 2001.

*Research Assistant, Mechanical Engineering Department, Thermosciences Division; currently Research Engineer, Spacecraft Propulsion Branch, Air Force Research Laboratory, Edwards Air Force Base, California 93524.

†Associate Professor, Mechanical Engineering Department, Thermosciences Division.

If an absorber has a velocity component u along the axis of the laser beam, it will absorb the light at a frequency shifted from that of stationary absorbers due to the Doppler effect. The magnitude of this frequency shift $\delta\nu_{12}$ depends on the speed u along the laser beam axis.

$$\delta\nu_{12} = \nu_{12}(u/c) \tag{1}$$

where c is the speed of light. The Doppler shift of an absorbers fluorescence profile away from the line center of ν_{12} stationary absorbers is in proportion to u (Ref. 7).

Xenon Spectroscopy

The nine stable isotopes of xenon, the propellant most commonly used in Hall thrusters, each have a slight difference in their electron transition energies due to their differences in mass.[8] The odd mass isotopes are further spin split due to nuclear magnetic dipole and electric quadrapole moments. Nuclei that have an odd number of protons and/or an odd number of neutrons possess an intrinsic nuclear spin $\boldsymbol{I}h/2\pi$, where $\boldsymbol{I}$ is integral or half-integral depending on whether the atomic mass is even or odd, respectively.[9] For nuclei with nonzero nuclear spin (angular momentum), there exists an interaction of the nucleus with the electron shell. This interaction leads to the splitting of levels with angular momentum $\boldsymbol{J}$ into a number of components, each corresponding a specific value of the total angular momentum $\boldsymbol{F}$ (Ref. 10). Details of how hyperfine spin splitting affects the spectra of xenon, and in particular with regard to the transitions studied here, are described elsewhere.[3]

For the results reported here, we probed the 823.2- and 834.7-nm electronic transitions of neutral and singly ionized xenon, respectively. The isotopic and nuclear-spin effects contributing to the hyperfine structure of the $6s[\frac{3}{2}]^0_2$–$6p[\frac{3}{2}]_2$ neutral xenon transition at 823.2 nm produce 21 spectral lines (Fig. 1a). Similarly, the $5d[4]_{7/2}$–$6p[3]_{5/2}$ xenon ion transition at 834.7 nm has a total of 19 isotopic and spin split components (Fig. 1b). The hyperfine splitting constants that characterize the variations in state energies are only known for a limited set of energy levels. These are available for the neutral 823.2-nm transition. However, the 834.7-nm xenon ion transition only has data on the nuclear spin splitting constants of the upper state, and no information is available on the transition-dependent isotope shifts.[11–13]

For velocity measurements, it is convenient to probe more accessible transitions for which there is incomplete knowledge of the isotopic and nuclear-spin splitting constants. Manzella has previously used the $5d[4]_{7/2}$–$6p[3]_{5/2}$ xenon ion transition at 834.7 nm to make velocity measurements in a Hall thruster plume.[14] A convenient feature of this transition is the presence of a relatively strong line originating from the same upper state ($6s[2]_{3/2}$–$6p[3]_{5/2}$ transition at 541.9 nm), which allows for nonresonant fluorescence collection.[15] A nonresonant fluorescence scheme is preferred where there is the possibility of laser scattering from internal surfaces of the discharge.

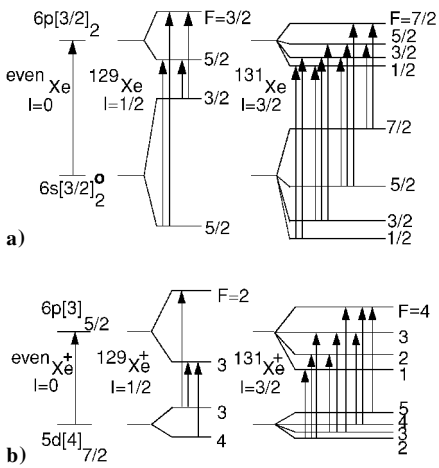

Fig. 1 Nuclear spin splitting of the a) neutral xenon $6s[\frac{3}{2}]^0_2$–$6p[\frac{3}{2}]_2$ and b) singly ionized xenon $5d[4]_{7/2}$–$6p[3]_{5/2}$ transitions.

Plasma Potential Measurements

When an electrically isolated conductor is placed in contact with a plasma, the more mobile electrons are depleted in the sheath region near the probe surface. The resulting electron retarding sheath causes the conductor to float at a potential ϕ_f lower than the plasma potential ϕ_p (Ref. 16). One method that is commonly used to measure the plasma potential is to heat a probe until a sufficient number of electrons are thermionically emitted from the probe surface to neutralize the sheath. Ideally, a neutralized sheath allows the probe to float at the local plasma potential. The advantage of using such an emissive probe is in its simplicity in design and interpretation of results. It avoids the interpretation of swept probe current-voltage characteristics in a plasma with a significant magnetic field for which present theory is inadequate, or in which electron saturation is difficult to achieve. Emissive probes also avoid the issues associated with the presence of impurity layers, such as oxide layers, which are otherwise difficult to remove and distort the current-voltage characteristic.[17]

The relationship between the plasma potential and the floating potential can also be used to estimate the electron temperature T_e. This requires an analysis of the electron and ion transport to an electrically floating surface in contact with the local plasma. If we assume that the probe electron flux is retarded by the difference potential between the floating and the plasma potentials ($\phi_f - \phi_p$) and that the ion current is limited by the Bohm current at the sheath edge, then equating the electron and ion fluxes gives[17]

$$\phi_f - \phi_p = -(kT_e/e)\,\ell n[M/2\pi m_e]^{\frac{1}{2}} \tag{2}$$

where k is the Boltzmann constant, M is the ionic mass, m_e is the electron mass, and e is the elementary charge. It is seen from Eq. (2) that measurements of the plasma and floating potentials directly yield the electron temperature. The spatial variation in the plasma potential may be differentiated to yield the electric field $\boldsymbol{E}$.

Experiment

Test Facility

The Stanford high vacuum test facility consists of a nonmagnetic cylindrical stainless steel vessel approximately 1 m in diameter and 1.5 m in length. The facility is pumped by two 50-cm diffusion pumps mounted on the ends of the chamber. The diffusion pumps are backed by a 425 l/s mechanical pump. Figure 2 shows a schematic of the vacuum chamber. The base pressure with no flow is approximately 10^{-6} torr as measured by an ionization gauge calibrated for nitrogen. Chamber background pressures were approximately 10^{-4} torr (3×10^{-5} torr on xenon, $\pm 50\%$) during testing. Propellant flow to the Hall thruster anode and cathode is throttled by two Unit Instruments 1200 series mass flow controllers factory calibrated for xenon. The propellant used in this study was research grade (99.995%) xenon.

The thruster is mounted on a two-axis translation system. In the vertical, the thruster has a range of travel of approximately 30 cm. In the axial, or horizontal, direction, the thruster is constrained to a total travel of approximately 8 cm. Both stages have resolutions on the order of 10 μm. Although the repeatability is considerably courser, it is still significantly less than the dimensions of the laser

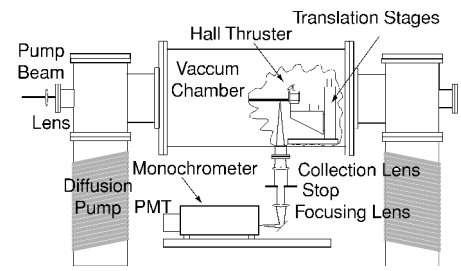

Fig. 2 Stanford high vacuum facility, collection optics, and LIF probe beam access for axial velocimetry with a cutaway view showing mounted Hall thruster.

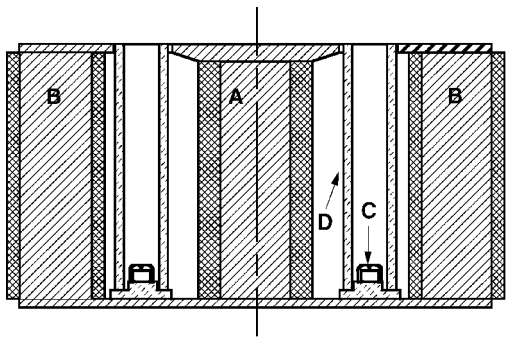

Fig. 3 Cross section of the Stanford Hall thruster: A) is the central iron core, B) the outer iron cores, C) the anode and propellant distribution system, and D) the alumina insulator.

probe volume in the axial dimension (approximately 100 μm diameter by 2 mm long). For internal LIF measurements, the thruster is mounted on a platform supported by the axial translation stage and a linear ball bearing pillow block. A cut out of the platform provides optical access through the slot in the outer thruster insulator into the acceleration channel from below. A view of the thruster mounting scheme is shown in Fig. 2.

Hall Thruster

The thruster used in this study has been described elsewhere.[18] It has 4 outer magnetic windings consisting of 89-mm-long, 25-mm-diam cores of commercially pure iron wrapped with 6 layers of 22 gauge Kapton® insulated copper magnet wire. The inner core is 25 mm in diameter and 89 mm in length and has 12 layers of magnet wire. The depth of the electrical insulator is 84 mm. The insulator is constructed from two sections of cast 99.9% alumina tubing cut to length. These two pieces are cemented to a machinable alumina plate attached to the back plate of the thruster with nonconducting fasteners. The thruster acceleration channel has an outer diameter of 95 mm and a 12 mm width. A cross-sectional view of the thruster is shown in Fig. 3. Not shown in Fig. 3 is the external hollow cathode neutralizer. The cathode used to neutralize the ion beam and sustain the anode discharge is an Ion Tech, Inc., HCN-252 hollow cathode capable of supporting a maximum 5-A emission current. It is mounted to the rear of the thruster on a stainless steel bracket such that the plane of the cathode exit is 20 mm beyond the thruster exit plane.

For this effort, a second insulator was constructed. It is identical to the insulator just described with the addition of a slot approximately 1 mm wide along the length of the outer wall cut with a diamond saw before assembly. The slot provides optical access to the interior of the Hall thruster. Operation of the Hall thruster with the slotted insulator does not differ significantly from the operation with the unslotted insulator. The current-voltage characteristics are identical. The slot width was selected to be less than the local electron Larmor radius to minimize its influence on the discharge properties. Despite the presence of the slot, optical access to the interior is still limited near the exit plane by the front plate of the magnetic circuit, precluding optical measurements very near the exit plane. The front iron plate is not cut because this would modify the local magnetic field.

LIF

The experimental apparatus used for the LIF measurements has also been described in detail elsewhere.[3] It consists of a tunable Coherent 899-21 single-frequency titanium sapphire laser, actively stabilized to provide linewidths on the order of 1 MHz with near-zero frequency drift. Scan widths of up to 20 GHz can be realized at center wavelengths between 680 and 1060 nm. The titanium sapphire laser is pumped by a Coherent Nd:YAG solid state Verdi® pump laser. The tunable laser wavelength is monitored by a Burliegh Instruments WA-1000 scanning Michaelson interferometer wavemeter with a resolution of 0.01 cm^{-1}. A schematic of the laser system is shown in Fig. 4.

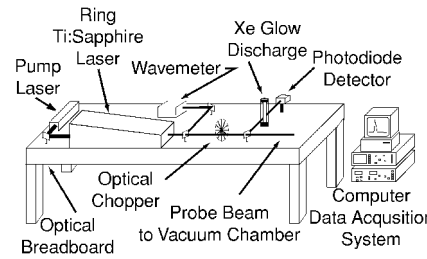

Fig. 4 LIF laser system and apparatus.

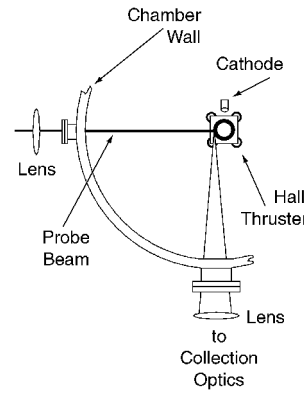

Fig. 5 LIF probe beam access for radial velocimetry.

The probe beam is chopped to allow for phase sensitive detection and is directed into the Hall thruster plume by a series of mirrors. For axial velocimetry measurements, the beam is focused to a submillimeter beam waist by a 50-mm-diam, 1.5-m focal length lens as shown in Fig. 2. For radial velocimetry measurements, the probe beam enters through a side window and is focused by a 50-mm-diam, 50-cm focal length lens as shown in Fig. 5. The collection optics for both radial and axial velocity measurements consist of a 75-mm-diam, 60-cm focal length, collimating lens. The collected light is then focused on to the entrance slit of a 0.5-m Ebert-Fastie monochrometer with a 50-mm-diam, 30-cm focal length lens. An optical field stop is placed between the two lenses to match the f-number of the optical train with that of the monochrometer, which acts as a narrowband optical filter so that only light from the transition of interest is collected. With entrance and exit slits fully open (425 μm), the 600-groove/mm plane grating (blazed for 600 nm) within the monochrometer allows the exit slit mounted Hamamatsu R928 photomultiplier tube to sample a wavelength interval of approximately 1 nm. The orientation of the monochrometer allows the slit aperture to define the length of the probe beam along which the fluorescence is collected. The sample volume for the axial data presented in this work is approximately 100 μm in diameter and 2 mm in length. Similarly, the sample volume of the radial data is approximately 100 μm in diameter and 1 mm in length. During neutral xenon LIF velocimetry measurements, a portion of the probe beam is split from the main beam, passed through a xenon glow discharge tube, and used as an stationary absorption reference. A silicon photo-diode monitors the absorption signal. The glow discharge does not support a sufficient population of excited state ions; therefore, use of the glow discharge tube is only possible for neutral xenon. However, the unshifted ion transition line center was confirmed by the expectation of very slow moving ions near the anode and by radial measurements near the acceleration channel center.

The LIF signal is collected using a Stanford Research Systems SRS-850 digital lock-in amplifier, whereas the absorption signal from the stationary reference is collected using an SRS-530 lock-in amplifier. Data from the absorption signal, laser power output, and the wavemeter are stored on the digital lock-in amplifier using three available analog inputs along with the LIF signal. Typical tests consist of a 12–20 GHz scan of the probe laser frequency over a 3-min period. The probe beam is chopped by an SRS-540 optical chopper at a frequency of 1.5 kHz. Both lock-in amplifiers use 1-s

time constants. Data are sampled at 8 Hz, producing four traces of approximately 2000 points for each velocity data point. Several unsaturated traces using lower laser intensities (less than 10 W/cm^2), 10-s time constants, and 10-min scans were also collected.

Plasma Potential Measurements

A schematic of the plasma potential probe used in this study is shown in Fig. 6. The probe body is a 6.35-mm-diam multibore mullite tube. Two 500-μm-diam tantalum leads jacketed by the mullite tube electrically connect the 150-μm-diam, 2% thoriated tungsten filament to the external power circuit. The filament is formed by winding the thoriated tungsten wire 8 turns around a 0.9-mm mandrel for a total length of approximately 1 cm. The filament is suspended between the two tantalum leads with a separation of 5 mm. During measurements, the filament coil axis is oriented to the $\boldsymbol{E} \times \boldsymbol{B}$ (azimuthal) direction within the discharge channel.

Figure 6 also shows a schematic of the probe electrical circuit. The probe is heated using a 10:1 step down transformer powered by a 10-A variable transformer connected to wall current (120-V ac, 60 Hz). This transfers current to the probe while allowing the probe circuit to float at the plasma potential. The current heating the probe is monitored by an ammeter to ensure repeatability of the measurements. The plasma potential is measured by a voltmeter relative to the thruster ground (connected to an Earth ground through the vacuum chamber). The emissive plasma potential probe is similar to those used by Morozov et al.[19] in a previous Hall thruster study.

The probe was mounted on a translation stage that allowed motion of the probe into the thruster acceleration region. A typical test procedure consisted first of moving the probe into the plasma region of interest. At this time, the floating potential of the plasma would be recorded. Subsequently, a current of 4 A heated the probe for approximately 5 s at which time the high-temperature floating potential (plasma potential) would be recorded. The probe current would then be turned off, and the probe would be moved to a new position to interrogate a new portion of the plasma. Because of the width of the probe, measurements within the thruster were limited to the channel center.

The plasma potential measurements are found to have a repeatability of approximately ± 3 V. A study of the variation in the measured probe potential with current (ac) through the probe filament (see Fig. 7) suggests that the measurements are accurate to within approximately 3 V of the plasma potential. Because the spatial measurements reported in this work were taken at a fixed filament current (4 A), the estimated uncertainty in the reported plasma potential is $-3/+6$ V. The related uncertainty of the electron temperature can be calculated from the uncertainty associated with the measurement of the plasma and the floating potentials and is approximately ± 0.5 eV. With the use of the Bohm criterion Eq. (2), the calculated electron temperatures should be viewed as a lower bound to the true electron temperature.

Note that, at 100 V, the lowest discharge voltage examined, the discharge current does not appreciably vary during insertion and removal of the probe (<8%). In all cases, the discharge current does not vary when the probe is heated. At higher discharge voltages, the discharge current is strongly affected by the position of the 6-mm-diam probe within the acceleration channel. For all cases above 160 V when the probe tip is traversing the first 20 mm within the acceleration channel, the discharge current rises to nearly 130% of the nominal value. Placing the probe further into the thruster beyond 20 mm, raises the potential an additional 10%, or less. This effect is not seen during 100-V operation.

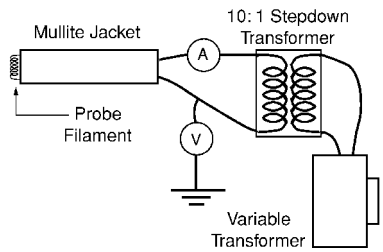

Fig. 6 Emissive plasma potential probe and power circuit.

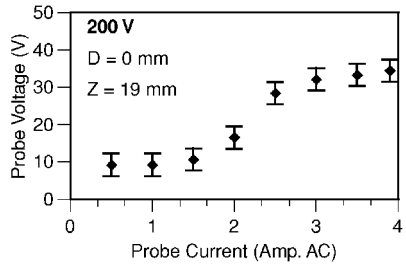

Fig. 7 Emissive plasma potential probe floating characteristics at $Z = 13$ mm, $D = 0$ mm at a discharge voltage of 200 V.

Results and Analysis

The Hall thruster was operated at four conditions for the work reported here. At each condition, the peak magnetic field was 125 G, the mass flow to the anode was 2.0 mg/s, and the mass flow to the external hollow cathode was 0.3 mg/s. The test conditions corresponded to discharge voltages of 100, 160, 200, and 250 V. The anode currents for these conditions are 2.1, 2.4, 2.6, and 2.9 A, respectively. The total power consumed by the cathode and magnet circuit was approximately 30 W.

All spatially resolved measurements are referenced to a two coordinate system shown in Fig. 8. The position in the radial coordinate is referenced to the radial midpoint of the acceleration channel using the variable D, defined as positive toward the thruster centerline. The axial coordinate is given by Z, which is the distance from the thruster exit plane, and is defined as positive along the thrust vector.

Xenon Ion LIF Velocimetry

The axial LIF velocimetry measurements consist of two data sets for each operating condition. The first data set consists of ion velocity measurements taken externally extending from the exit plane to approximately $Z = 35$ mm. The second data set contains internal axial velocity measurements taken from the exit plane to approximately $Z = -75$ mm. These ranges are imposed by the limited travel of the translation stage that provides axial motion to the Hall thruster. Axial velocimetry measurements were taken every 2.5 mm with a sample probe volume of 100 μm in diameter and 2 mm long. For several of the test conditions examined, profiles of the axial velocity across the coordinate D were also examined. Measurements of near plume radial velocities were also performed. These measurements are limited to the plume due to the limited optical access to the interior of the Hall thruster.

The complete axial velocity profiles for the four cases examined are shown in Fig. 9. The error bars correspond to the ± 500 m/s uncertainty associated with the determination of the magnitude of the Doppler shift relative to the unshifted line center. The axial velocity profiles exhibit the expected behavior. The velocity is near zero close to the anode ($Z = -78$ mm), and begins to rise at $Z = -10$ mm at the edge of the acceleration zone. The ions are rapidly accelerated in the region of the exit plane and reach their full velocity in the neighborhood of $Z = 20$ mm. This position corresponds to the location

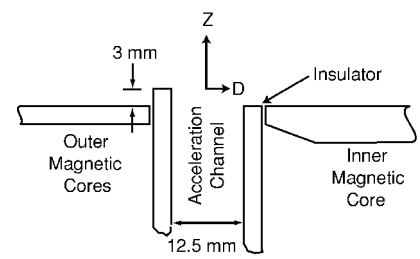

Fig. 8 Coordinate system for referencing locations of measurements.

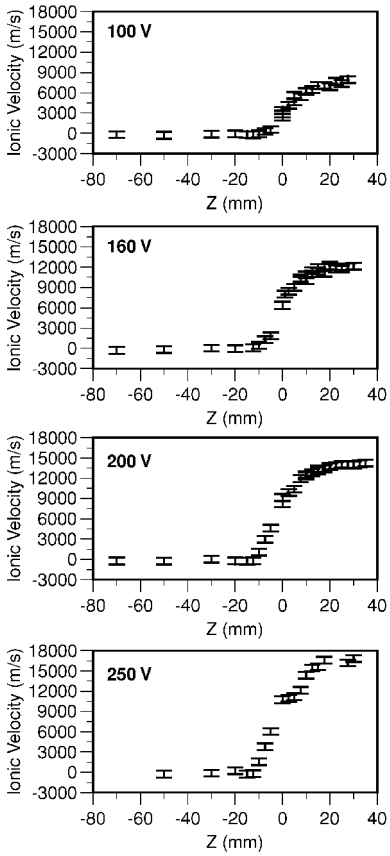

Fig. 9 Axial xenon ion velocity measurements at $D = 0$ mm for discharge voltages of 100, 160, 200, and 250 V.

of the hollow cathode neutralizer relative to the body of the thruster and is sometimes referred to as the cathode plane in the literature.[14]

The length of the acceleration region in all cases is invariant at 30 mm. Therefore, increases in the anode potential result in a concomitant increase of the axial electric field component within the acceleration channel. The initial acceleration is seen to begin at 10 mm within the thruster where the magnetic field has a value of approximately 85% of the centerline maximum. The propellant acceleration is completed 20 mm beyond the exit plane when the magnetic field has a value of approximately 25% of the centerline maximum.

Significant acceleration of the ionized propellant occurs outside the Hall thruster. This is consistent with the results first identified in a Hall discharge with a much shorter acceleration channel (see Ref. 2). The velocity increment imparted to the propellant outside of the Hall thruster is essentially constant, is invariant with discharge voltage, has an average value of 5000 m/s. Only for the 100-V case does the majority of the acceleration occur outside the thruster. Higher discharge voltages appear to have a constant percentage of the acceleration occurring externally. It is more informative to cast this result in terms of the kinetic energy deposited into the propellant. In the case of the 100-V discharge operation, approximately 90% of the energy is deposited into the propellant between the exit and cathode planes. For the 250-V case, the fraction of energy deposition beyond the exit plane is nearer to 60%. The majority of the energy deposition into the Hall thruster propellant occurs outside the thruster. However, because the thrust is proportional to the momentum flux, rather than the energy flux, the majority (65%) of the thrust is still generated within the thruster in all cases above 100 V. Note that in all cases approximately 60 eV is unaccounted. This value is constant to within the uncertainties of the velocity measurement and implies that the mechanism responsible for this loss is invariant with the applied anode potential. This energy loss may be a product of the anode and cathode potential falls, or other mechanisms common to these discharges, for example, distribution of ion production

Table 1 Ion acceleration characteristics

Property	100 V	160 V	200 V	250 V
Exit plane				
Velocity, m/s	2,900	8,000	9,200	10,800
Energy, eV	5	44	58	79
Maximum				
Velocity	8,000	12,200	14,200	16,800
Energy	44	102	138	191
External acceleration, m/s	5,100	4,200	5,000	6,000
(% of maximum)	(65)	(35)	(35)	(35)
External energy, eV	39	58	80	112
(% of maximum)	(90)	(55)	(60)	(60)
Lost energy, eV	56	58	62	59
(% applied voltage)	(55)	(35)	(30)	(25)

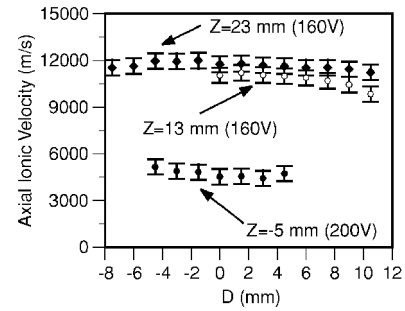

Fig. 10 Radial profiles of axial xenon ion velocity measurements for several discharge voltages and locations.

region, or resistive losses in regions of low ionization fractions. These results are summarized in Table 1. Note that these measurements are limited to axial velocities, and plume divergence is not considered.

Several radial profiles of the axial ion velocity in Fig. 10 illustrate the radial variation of the measured axial velocities for a discharge voltage of 160 V at two locations in the plume and one within the thruster for a discharge voltage of 200 V. The axial velocity profile is nearly flat, which strongly implies lines of constant potential in the radial direction. The slightly concave distribution inside the channel (200-V case) is consistent with the expected equipotential surfaces associated with the radial magnetic field.

Radial velocity measurements were also performed in the plume. Shown in Fig. 11 are radial measurements for the four operating conditions at an axial position $Z = 13$ mm. The flow exiting the Hall thruster is highly divergent. The propellant stream has a substantial radial velocity, especially away from the center of the acceleration channel. The profile is symmetrical and linear with the acceleration channel center, $D = 0$ mm, where the radial velocity is near zero. Combined with the preceding axial velocity measurements and the knowledge that the axial velocity is independent of D, vector plots of the near plume may be constructed. Figure 12 shows a vector plot constructed for the 200-V case. Here the radial velocities vary linearly with D with peak values above 6000 m/s as close as $Z = 13$ mm and $D = 8$ mm. A prominent feature of a Hall thruster plume is the luminous central cone originating at the thruster axis adjacent to the center pole piece. Although the propellant stream exits the thruster in an annulus, an intense, optically emitting conical feature extends a significant distance into the vacuum chamber (10–30 cm for our background pressures) and is especially evident at higher discharge voltages. The inward focus of the divergent propellant flow is likely a contributing mechanism in the formation of this intriguing feature, which is not precisely understood.

Ion Line Shape Analysis

The hyperfine splitting constants for the xenon ion $5d[4]_{7/2}$–$6p[3]_{5/2}$ transition at 834.7 nm are only known for the upper $6p[3]_{5/2}$ state. The isotope shifts for this transition are also unknown. Although this does not greatly impact the accuracy to which velocities

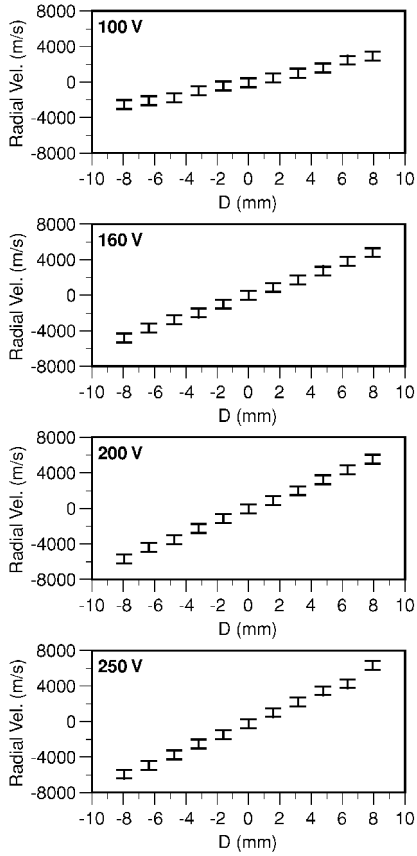

Fig. 11 Radial profiles of radial xenon ion velocity measurements for several discharge voltages at $Z = 13$ mm.

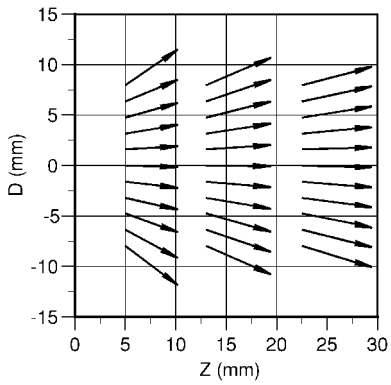

Fig. 12 External xenon ion velocity field calculated from radial and axial velocity measurements for a 200-V discharge voltage.

may be determined, it does impact the ability to use this transition for accurate measurements of the ion velocity distribution, or temperature. Note that the notion of a temperature for the ions in this flow is highly tenuous because the ions may be treated kinetically, do not suffer many collisions, and are created at distributed axial locations within the discharge. Furthermore, a time-averaged broadening of the fluorescence excitation spectra can arise due to oscillations in the zone of ionization. King[20] has shown by mass and resolved energy analysis that the axial velocity of the ions has an energy distribution of approximately 10 eV (in the far field) due in part to the plasma oscillations within the Hall thruster. The issue of the distribution of ion velocities due to the axial location where they were created is minimized by examining the fluorescence spectra in the radial direction at a location with near-zero radial velocity. The spectra are taken from the position with the minimum measured velocity, approximately 100 m/s (±500 m/s) at a location of $D = 0$ mm and $Z = 13$ mm. For a temperature to be extracted from the measured

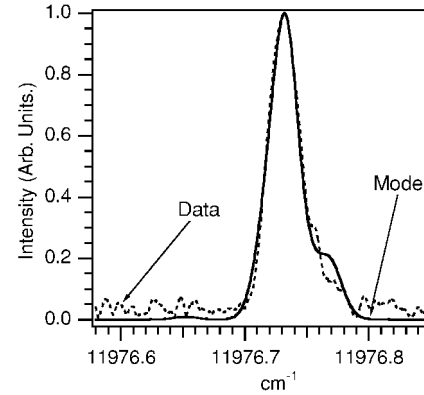

Fig. 13 Model fit to unsaturated radial fluorescence trace at a discharge voltage of 200 V at $D = 0$ mm and $Z = 13$ mm.

line shape, the ion population is assumed to be Maxwellian, or at least frozen in a close facsimile. In addition, the line shape is assumed to be primarily Doppler broadened.

An estimate of the ion kinetic temperature with uncertainties of 40–70% is possible. A radial excitation unsaturated fluorescence trace is shown in Fig. 13 and compared to a line shape model developed by Cedolin.[21] The model uses the $5d[3]_{7/2}$ lower level hyperfine spin splitting and isotopic shift data from the 605.1-nm transition and the measured splitting data for the upper $6p[3]_{5/2}$ level. Lorentzian broadening is neglected, and only Doppler broadening is considered. The best fit of this model predicts a kinetic temperature of approximately 450 K. The model does not completely predict the outlying features, but this is expected because the spin splitting constants for the $5d[3]_{7/2}$ state are used for the lower level rather than those for the $5d[4]_{7/2}$ state probed here. A check of the uncertainty of the preceding analysis may be performed by variously simplifying to the line shape model. If hyperfine splitting is ignored and only the isotope shifts corresponding to the values for the 605.1-nm transition are used, the model predicts a kinetic temperature of approximately 800 K. Finally, by neglecting all hyperfine splitting mechanisms, including isotopic and nuclear-spin splitting, an absolute maximum temperature of 1700 K is determined from the fluorescence Doppler half-width. The uncertainty of this measurement is in large part due to the uncertainties of the spectral data, as well as due to the noise in the fluorescence signal. A similar measurement in the plume of a stationary plasma thruster (SPT-100) by Manzella[14] yielded a kinetic temperature of approximately 800 K. Note that Manzella used an incorrect value of J for the lower state, which was first misidentified by Humphreys[22] and propagated by Moore[23] before finally being corrected by Hansen and Persson.[15]

Neutral LIF Velocimetry

Figure 14 shows the results of axial neutral xenon velocity measurements within the acceleration channel. The four cases examined show very similar behavior. The initial velocity near the anode is very low. The neutral velocity slowly rises until a position of approximately 20 mm within the thruster. At this point, where the ion acceleration is also seen to begin, the neutrals are accelerated at a higher rate until near the exit plane where the acceleration appears to slow and even possibly reverse when the thruster is operated at higher voltages. The decrease in neutral xenon velocity is likely due to thruster ingestion of background xenon. Because the effect appears to grow with increased discharge voltage, it is possible that a portion of the propellent flow reflected from nearby vacuum facility walls (now entirely consisting of neutrals) is ingested by the thruster.

Because of the highly nonequilibrium nature of the Hall thruster, it is important to understand the apparent acceleration of the neutrals beginning 40 mm upstream of the exit plane. The plasma within the Hall thruster is required to be of low collisionality by the constraint that the magnetic field limit the electron flux to the anode. The disparate velocities of the ions and neutrals strongly suggest that the

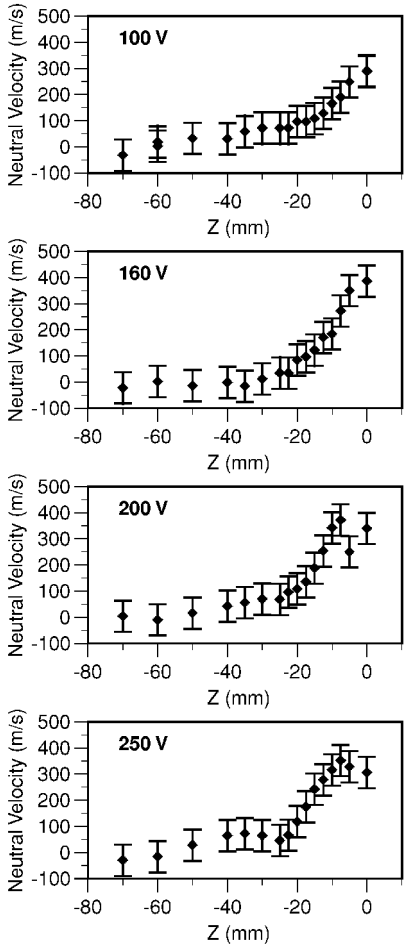

Fig. 14 Axial neutral velocity measurements at $D = 0$ mm for discharge voltages of 100, 160, 200, and 250 V.

neutral and ion populations are not coupled. As such, the apparent acceleration of the neutrals may actually be an artifact of their time of flight through the volumetric zone of ionization. Slower neutrals have a greater probability of being ionized than do neutrals in the high-energy portion of the velocity distribution. Therefore, neutrals from the high-energy range of the velocity distribution are more likely to reach the upstream portion of the acceleration channel. In this case, there is not an actual acceleration of the neutrals, but rather a depletion of the slower moving neutrals by ionization.

The depletion of the slower neutral velocity classes accounting for the apparent acceleration of the neutrals as seen in Fig. 14 may be qualitatively explained by considering the one-dimensional Boltzmann equation (see Ref. 24):

$$u\frac{\partial}{\partial z}[nf(u)] = -[nf(u)]n_e S_i \tag{3}$$

where n is the neutral number density, u is the neutral velocity class, z is the spatial coordinate, $f(u)$ is the velocity distribution function, n_e is the local plasma electron number density, and S_i is the ionization rate coefficient. The generalized one-dimensional Boltzmann equation is simplified here by assuming the process is steady with no external forces and that the sole depletion mechanism for the neutral velocity classes is electron collisional ionization.

Equation (4) may be easily integrated with respect to $nf(u)$ to produce an analytic solution if the ionization rate coefficient S_i and the electron number density n_e are assumed to be constant. In this case, the population of the u velocity class $nf(u)$ exponentially decays with the spatial variable z moderated by the value of u:

$$nf(u) \sim \exp(-z/u) \tag{4}$$

The qualitative conclusion drawn from this straightforward analysis of the one-dimensional Boltzmann equation is that the neutral density in a model plasma is depleted along the Z axis due to neutral–electron collisional ionization. This relative depletion depends on the velocity class. Neutrals in the lower velocity classes have a greater probability of being ionized when passing through the zone of ionization than neutrals of higher velocity classes. Therefore, the apparent acceleration of the neutrals in Fig. 14 is most likely the result of the depletion of the slower moving neutrals rather than an acceleration process.

Plasma Potential Measurements

Because Hall thrusters are electrostatic accelerators, knowledge of the plasma potential is important in understanding the propellant acceleration process. A comparison between the ion velocity measurements and the plasma potential measurements provides an insight into the dynamics and ionization processes within the acceleration channel.

Figure 15 shows the measured axial plasma potential and electron temperature for the four test conditions. Each data trace shows similar behavior where the potential is constant in the far plume near a value of 25 V. As the probe traverses into the thruster acceleration channel, the potential rises significantly as the impedance of the radial magnetic field to the axial electron current is encountered. The plasma potential has reached 80–90% of the anode potential by $Z = -20$ mm. The remaining 10–20% of the potential is distributed between this position and the anode and is a major inefficiency as few ions are produced here. The 250 V case is incomplete due to failure of the probe.

The electron temperature calculated using Eq. (2) is also shown in Fig. 15. The electron temperature is at a relatively low value (2.5–3 eV) in the plume and rises with the rising plasma potential to a maximum located between $Z = -8$ and -10 mm. The electron

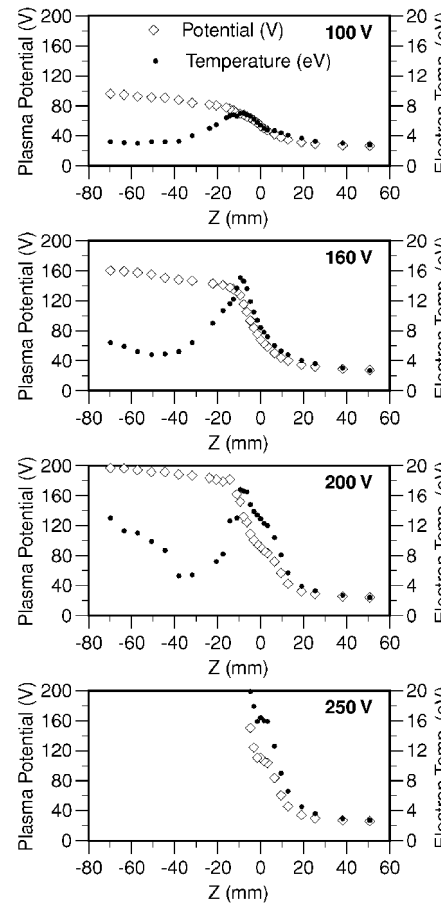

Fig. 15 Axial profiles of plasma potential (+6/− 3 V) and electron temperature (± 0.5 eV) at $D = 0$ mm.

temperature then begins to fall even though the plasma potential is only at 80% of the anode potential. Closer to the anode ($Z < -40$ mm), the electron temperature again begins to rise. This effect becomes more pronounced as the discharge voltage increases. For a 100-V discharge, the electron temperature rise near the anode is nearly imperceptible. At 160 V, the rise is well defined, and at 200 V, the rise in electron temperature near the anode approaches the peak temperatures of the exit plane.

There have been reports of similar electron temperature behavior in Hall discharges. In a study by Morozov et al.,[19] a two-dimensional potential field of a Hall thruster of similar geometrical dimensions operating on argon at a discharge voltage of 400 V was mapped.[19] Strong variation in the radial direction of the plasma potential was found in the 30 mm nearest to the anode within an acceleration channel of 138-mm total length. Such measurements were not possible on the Stanford Hall thruster due to relative sizes of the probe body and acceleration channel; however, a similar potential field is implied in this case because it would produce a radial electric field near the anode that would heat local electrons to the elevated temperatures seen in Fig. 15.

Radial profiles of the plasma potential and the derived electron temperature at $Z = 13$ mm are shown in Fig. 16. The data show a portion of the structure within the near-field plume. The asymmetry is indicative of the development of the bright central core feature. This asymmetry manifests itself the greatest at low discharge voltages, where the potential near the central magnetic core remains at a higher value than it does toward the periphery (lesser values of D). This phenomenon lessens at higher discharge voltages; however, the difference between the potentials within the core and those in the outer portion of the plume remains approximately 10 V in all cases. Less mixing is occurring as the ionized propellant stream has greater momentum with increased discharge voltage. This may

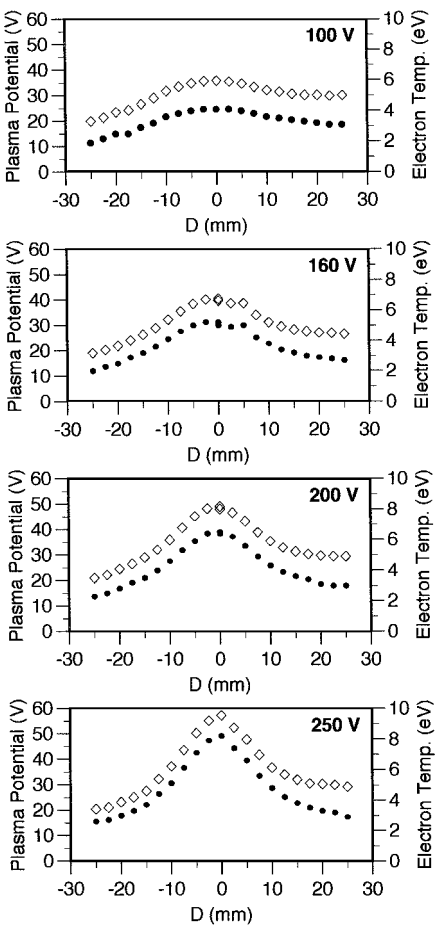

Fig. 16 Radial profiles of plasma potential (+6/− 3 V) and electron temperature (± 0.5 eV) at Z = 13 mm.

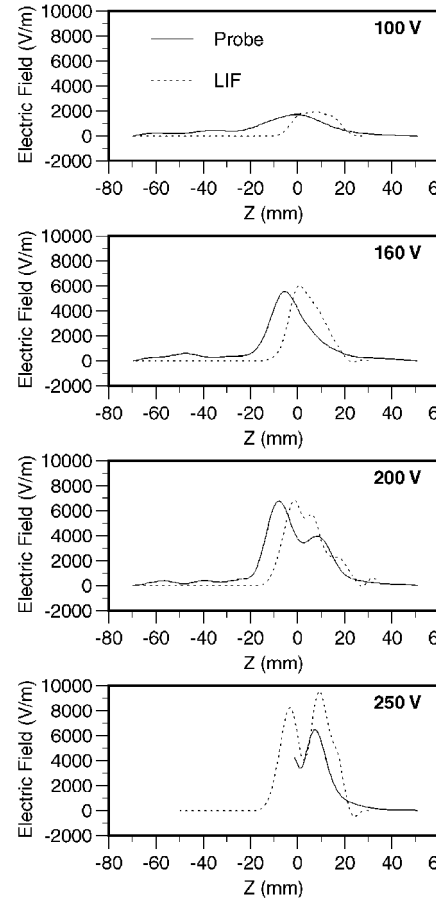

Fig. 17 Axial electric field components calculated from plasma potential measurements and from LIF velocimetry measurements at $D = 0$ mm.

explain the extended plume structure seen at the higher discharge voltages. The electron temperature data exhibit similar asymmetry to the plasma potential data, especially at the lower discharge voltages. However, this asymmetry is less pronounced than it is for the plasma potential data.

Electric Field Calculations

The axial component of the electric field shown in Fig. 17 is derived from the plasma potential data in Fig. 15. Figure 17 also presents the electric field calculated by determining the ion kinetic energy from the velocimetry data in Fig. 9 then differentiating to produce an effective electric field. The two data sets are similar indicating that the ionization and acceleration regions within the thruster are separated to some degree. The differences between the two sets of curves are due to the differences between the measurements. Ion creation occurs in a volume and, therefore, the LIF-derived plasma potentials are only valid beyond the region of ion creation that appears to lie near $Z = -10$ mm. There is some ionization occurring throughout the acceleration channel. Some ions are created in regions where the electric field is high, and this masks the detection of local electric fields using velocimetry data, especially if the ion creation region is large and the ion velocities are distributed. For the plasma potential probe, the primary source of uncertainty is the degree of disturbance. The LIF velocimetry is less intrusive with only the addition of the slot in the insulator.

Although both data sets in Fig. 17 show similar trends, some of the features are different, particularly those more than 10 mm within the Hall thruster exit plane. Between $Z = -10$ mm and the anode, there exists only a small population of ions with low axial velocities with uncertain creation and loss rates. Velocimetry studies prove inadequate to study the potential and electric field in this region, but potential probe measurements, assuming that they do not

significantly perturb thruster operation, provide better measurement of the electric field. Near the exit plane, it is likely that the probe masks the higher gradients of the plasma potential due to the perturbation of the plasma flowfield.

Both general trends agree, particularly near the exit plane where a dip in the electric field is apparent. This sudden change in the shape of the electric field near the exit plane is visible in both data sets and increases with discharge voltage. When it is assumed that the axial current is a constant and because the local radial magnetic field is continuous, the dips in the electric field are attributed to changes in the local plasma conductivity indicating a sharp drop in the electron temperature, a rise in the electron density, or plasma fluctuations. The measured electron temperature does not support the former. A sharp rise in the electron density is probably not indicated because the plasma density should decrease with increasing discharge voltage due to the increased ion velocity. Plasma oscillations have already been shown to be the cause of so-called anomalous diffusion of electrons through magnetic field lines.[25,26] A recent study has shown that significant plasma density oscillations with a characteristic frequency of approximately 10 kHz occur near the exit plane.[27] These oscillations are capable of increasing the local plasma conductivity and significantly lowering the electric field as shown in Fig. 17.

Figure 18 shows the radial component of the electric field calculated from the radial plasma potential measurements presented in Fig. 16. The radial electric field component peaks at a relatively large value and shows the electrostatic forces focusing/defocusing the plume. The radial electric field increases with discharge voltage from a peak value near 1000 V/m at 100 V operation to approximately 2500 V/m at a discharge voltage of 250 V. The peak value of the radial component of the electric field at this location in the plume is approximately equal to the axial component at this location. The variation of the radial electric field is similar to the variation seen in the axial component of the thruster magnetic field. The impedance

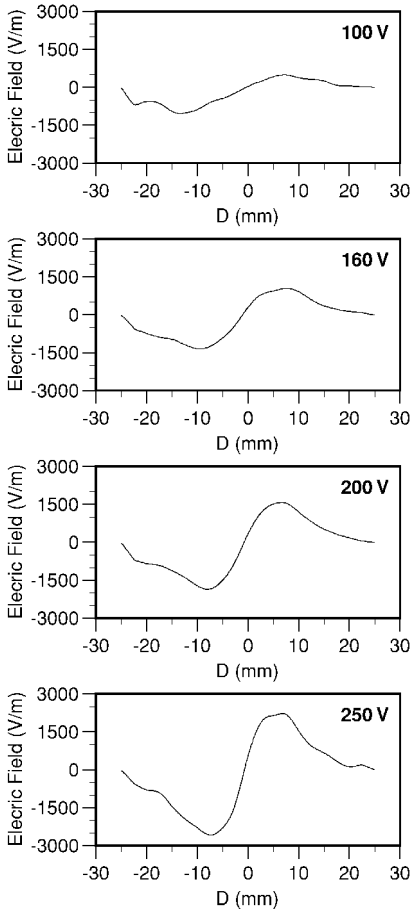

Fig. 18 Radial electric field components in the plume at $Z = 13$ mm.

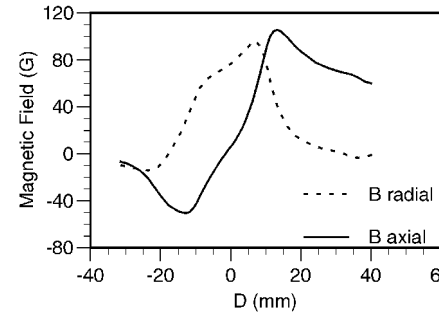

Fig. 19 Plot of the axial and radial components of the magnetic field (± 1 G) at $Z = 3$ mm.

of the plasma, whether either classical or enhanced electron diffusion holds, is a function of the magnetic field strength. Figure 19 is a plot of the magnetic field components at $Z = 3$ mm. The variation of the axial portion of the magnetic field is of most interest. The radial electric field appears to follow closely the behavior of the axial magnetic field. The effect of density may be visualized from the variation of discharge voltage. As the discharge voltage is increased, the velocity of the ion propellant stream rises and the plasma density falls. Along with the fall in plasma density, the conductivity falls and the radial electric field increases.

Conclusions

Measurements of xenon ion and neutral velocities were obtained in the plume and into the interior of the thruster through a 1-mm-wide slot in the outer insulator wall. From these measurements, information on propellant energy deposition, electric field strength, and flow divergence were extracted. Ion velocity measurements of axial velocity both inside and outside the thruster, as well as radial velocity measurements outside the thruster, were performed using LIF with nonresonant signal detection using the xenon ion $5d[4]_{7/2}$–$6p[3]_{5/2}$ electronic transition while monitoring the signal from the $6s[2]_{3/2}$–$6p[3]_{5/2}$ transition. Neutral velocity measurements were similarly obtained in the interior of the Hall thruster using the $6s[3/2]^0_2$–$6p[3/2]_2$ transition with resonance fluorescence collection. Most velocity measurements used partially saturated fluorescence to improve the signal-to-noise ratio. One radial trace of the ion transition was taken in the linear fluorescence region and yielded a plume ion translational temperature between 400 and 800 K. However, because the hyperfine structure constants are not known for the $5d[4]_{7/2}$ level, the constants for the $5d[3]_{7/2}$ level were used instead. This result should, therefore, be viewed with caution. An upper limit on the kinetic temperature using only the full width at half maximum assuming no hyperfine splitting yields a temperature of 1700 K. From the neutral velocity measurements, the neutrals appear to be accelerated within the thruster. Conclusions drawn from analysis of the one-dimensional Boltzmann equation imply that the neutral density in a model plasma is depleted along the Z axis due to neutral–electron collisional ionization and that the relative depletion depends on the velocity class of the neutral atom. This preferentially depletes the lower velocity classes producing the apparent acceleration of the neutrals.

Plasma potential measurements were made in the plume and interior of the thruster. The potential measurements showed that the far plume was approximately 25 V above ground, corresponding to the potential of the electrons produced by the hollow cathode neutralizer. Electric field values derived from the plasma potential measurements show that the fields are relatively smooth and peak near the exit plane. Maximum field strengths were found to approach 8000 V/m. At the exit plane, the axial electric fields show a dip that becomes more significant with increasing discharge voltage. This dip in the electric field may be due to the locally increased conductivity due to plasma oscillations. In addition, an estimate of the electron temperature was extracted at the location of each plasma potential measurement.

Acknowledgments

This work is supported by the Air Force Office of Scientific Research. W. A. Hargus Jr. was supported under the U.S. Air Force Palace Knight Program.

References

[1]Janson, S. W., "The On-Orbit Role of Electric Propulsion," AIAA Paper 93-2220, June 1993.

[2]Cedolin, R. J., Hargus, W. A., Jr., Storm, P. V., Hanson, R. K., and Cappelli, M. A., "Laser-induced Fluorescence Study of a Xenon Hall Thruster," *Applied Physics B: Lasers and Optics*, Vol. 65, No. 4/5, 1997, pp. 459–469.

[3]Hargus, W. A., Jr., and Cappelli, M. A., "Laser-Induced Fluorescence Measurements of Velocity within a Hall Discharge," *Applied Physics B: Lasers and Optics* (to be published).

[4]Capelli, M. A., Hargus, W. A., Jr., and Meezan, N. B., "Coherent Structures in Crossed-Field Closed-Drift Hall Discharges," *IEEE Transactions on Plasma Science*, Vol. 27, No. 1, 1999, pp. 96, 97.

[5]Storm, P. V., "Optical Investigations of Plasma Properties in the Interior of a Arcjet Thrusters," Ph.D. Dissertation, Thermosciences Div. Rept. TSD-102, Stanford Univ., Stanford, CA, 1997.

[6]Keefer, D., Wright, N., Hornkohl, J., and Bangasser, J., "Multiplexed LIF and Langmuir Probe Diagnostic Measurements in the TAL D-55 Thruster," AIAA Paper 99-2425, June 1999.

[7]Demtroder, W., *Laser Spectroscopy: Basic Concepts and Instrumentation*, Springer-Verlag, Berlin, 1996, pp. 829, 830.

[8]Herzberg, G., *Atomic Spectra and Atomic Structure*, Dover, New York, 1944, pp. 182–196.

[9]Cowan, R. D., *The Theory of Atomic Structure and Spectra*, Univ. of California Press, Berkeley, CA, 1981, pp. 505–511.

[10]Sobelman, I. I., *Atomic Spectra and Radiative Transitions*, Springer-Verlag, New York, 1992, pp. 159–170.

[11]Geisen, H., Krumpelmann, T., Neuschafer, D., and Ottinger, C., "Hyperfine Splitting Measurements on the 6265 Å and 6507 Å Lines of Seven Xe Isotopes by LIF on a Beam of Metastable Xe($^3P_{0,3}$) Atoms," *Physics Letters A*, Vol. 130, No. 4.5, 1988, pp. 299–304.

[12]Fischer, W., Huhnermann, H., Kromer, G., and Schafer, H. J., "Isotope Shifts in the Atomic Spectrum of Xenon and Nuclear Deformation Effects," *Zeitschrift für Physik*, Vol. 270, No. 113, 1974, pp. 113–120.

[13]Bronstrom, L., Kastberg, A., Lidberg, J., and Mannervik, S., "Hyperfine-structure Measurements in Xe II," *Physical Review A*, Vol. 35, No. 1, 1996, pp. 109–112.

[14]Manzella, D. H., "Stationary Plasma Thruster Ion Velocity Distribution," AIAA Paper 94-3141, June 1994.

[15]Hansen, J. E., and Persson, W., "Revised Analysis of Singly Ionized Xenon, Xe II," *Physica Scripta*, Vol. 36, No. 4, 1987, pp. 602–643.

[16]Chen, F. F., *Introduction to Plasma Physics and Controlled Fusion*, Vol. 1, Plenum, New York, 1990, pp. 290–297.

[17]Hershkowitz, N., "Theory of Electrostatic Probes," *Plasma Diagnostics*, Vol. 1, edited by O. Auicello and D. Flam, Academic Press, New York, 1989, pp. 113–183.

[18]Hargus, W. A., Jr., Cedolin, R. J., Meezan, N. B., and Cappelli, M. A., "A Performance Study of a Low Power Hall Thruster," AIAA Paper 97-3081, July 1997.

[19]Morozov, M. I., Esipchuk, Y. V., Tilinin, G. N., Trofimov, A. V., Sharov, Y. A., and Shepkin, G. Y., "Plasma Accelerator with Closed Electron Drift and Extended Acceleration Zone," *Soviet Physics—Technical Physics*, Vol. 17, No. 1, 1972, pp. 38–45.

[20]King, L. B., "Transport-Property and Mass Spectral Measurements in the Plasma Exhaust Plume of a Hall-Effect Space Propulsion System," Ph.D. Dissertation, Aerospace Engineering, Univ. of Michigan, Ann Arbor, MI, 1998.

[21]Cedolin, R. J., "Laser-Induced Fluorescence Diagnostics of Xenon Plasmas," Ph.D. Dissertation, Mechanical Engineering, Stanford Univ., Stanford, CA, June 1997.

[22]Humphreys, C. J., "Second Spectrum of Xenon," *Journal of the National Bureau of Standards*, Vol. 22, Jan. 1939, pp. 19–53.

[23]Moore, C. E., *Atomic Energy Levels*, Vol. 3, National Bureau of Standards, Washington, DC, 1958, pp. 113–123.

[24]Vincenti, W. G., and Kruger, C. H., Jr., *Introduction of Physical Gas Dynamics*, Krieger, Malabor, FL, 1986, p. 332.

[25]Yoshikawa, S., and Rose, D., "Anomalous Diffusion of a Plasma Across a Magnetic Field," *Physics of Fluids*, Vol. 5, No. 3, 1963, pp. 334–340.

[26]Meezan, N. B., Hargus, W. A., Jr., and Cappelli, M. A., "Anomalous Electron Mobility in a Coaxial Hall Plasma," *Physical Review E*, Vol. 63, 026410, 2001.

[27]Bouef, J., and Garrigues, L., "Low Frequency Oscillations in a Stationary Plasma Thruster," *Journal of Applied Physics*, Vol. 84, No. 7, 1998, pp. 3541–3554.